

 Open access • Posted Content • DOI:10.1101/552265

Biofilm structure promotes coexistence of phage-resistant and phage-susceptible bacteria — [Source link](#)

Matt Simmons, Matthew C. Bond, Britt Koskella, Knut Drescher ...+4 more authors

Institutions: University of Massachusetts Dartmouth, University of California, Berkeley, University of Marburg, Max Planck Society ...+1 more institutions

Published on: 08 Oct 2019 - bioRxiv (Cold Spring Harbor Laboratory)

Topics: Population and Biofilm

Related papers:

- [Biofilm Structure Promotes Coexistence of Phage-Resistant and Phage-Susceptible Bacteria.](#)
- [Evolutionary dynamics of phage resistance in bacterial biofilms](#)
- [Phage mobility is a core determinant of phage-bacteria coexistence in biofilms](#)
- [Bacteriophage exploitation of bacterial biofilms: phage preference for less mature targets?](#)
- [Theory for the spatiotemporal interaction between lytic phages and biofilm-dwelling bacteria](#)

Share this paper:    

View more about this paper here: <https://typeset.io/papers/biofilm-structure-promotes-coexistence-of-phage-resistant-4gblm1f8gu>

1 **Biofilm structure promotes coexistence of phage-resistant and** 2 **phage-susceptible bacteria**

3
4 Matthew Simmons^{1†}, Matthew C. Bond^{1†}, Britt Koskella², Knut Drescher^{3,4}, Vanni Bucci^{5*}, Carey D.
5 Nadell^{1*}

6
7 ¹ Department of Biological Sciences, Dartmouth, Hanover, NH 03755, USA

8
9 ² Department of Integrative Biology, University of California, Berkeley, Berkeley, CA 94720, USA

10
11 ³ Max Planck Institute for Terrestrial Microbiology, D-35043 Marburg, Germany

12
13 ⁴ Department of Physics, Philipps-Universität Marburg, D-35032 Marburg, Germany

14
15 ⁵ Department of Microbiology and Physiological Systems, University of Massachusetts Medical School,
16 Worcester, MA 01605, USA

17
18
19
20 † Co-first authors

21
22 * Authors for correspondence:

23
24 Carey Nadell (carey.d.nadell@dartmouth.edu)

25 Vanni Bucci (vanni.bucci2@umassmed.edu)

26

27 **Abstract**

28 Encounters among bacteria and their viral predators (bacteriophages) are among the most common
29 ecological interactions on Earth. Further, these encounters are likely to occur predominantly within
30 surface-bound communities that microbes most often occupy in natural environments. These
31 communities, termed biofilms, are spatially constrained such that interactions become limited to near
32 neighbors; diffusion of solutes and particulates is reduced; and there is pronounced heterogeneity in
33 nutrient access and physiological state. It is appreciated from prior, abstracted theory that phage-bacteria
34 interactions are fundamentally different in spatially structured contexts, as opposed to well-mixed liquid
35 culture. Spatially structured communities are predicted to promote the protection of susceptible host cells
36 from phage exposure, and thus weaken selection for phage resistance. The details and generality of this
37 prediction in realistic biofilm environments, however, are not known. Here we explore phage-host
38 interactions using experiments and simulations that are tuned to represent the essential elements of biofilm
39 communities. Our simulations show that in biofilms, the coexistence of susceptible and phage-resistant
40 bacteria is highly robust to a large array of conditions, including background growth rate, cost of phage
41 resistance, mechanism of phage resistance, and phage diffusivity. We characterize the population
42 dynamics underlying this coexistence, and we show that coexistence is recapitulated in an experimental
43 model of biofilm growth measured with confocal microscopy. Our results provide a clear view into the
44 dynamics of phage-resistance in biofilms, with single-cell resolution of the underlying cell-virion
45 interactions, linking the predictions of canonical theory to realistic models and *in vitro* experiments of
46 biofilm growth.

47

48 **Importance**

49 In the natural environment, bacteria most often live in communities bound to one another by secreted
50 adhesives. These communities, or biofilms, play a central role in biogeochemical cycling, microbiome
51 functioning, wastewater treatment, and disease. Wherever there are bacteria, there are also viruses that
52 attack them, called phages. Interactions between bacteria and phages are likely to occur ubiquitously in
53 biofilms. We show here, using simulations and experiments, that biofilms will almost universally allow
54 phage-susceptible bacteria to be protected from phage exposure, if they are growing alongside other cells
55 that are phage-resistant. This result has implications for the fundamental ecology of phage-bacterial
56 interactions, as well as the development of phage-based antimicrobial therapeutics.

57 **Introduction**

58 Because of the sheer number of bacteria and phages in nature, interactions between them are very common
59 (1–9). The imperative of evading phages on the part of their bacterial hosts – and of accessing hosts on
60 the part of phages – has driven the evolution of sophisticated defensive and offensive strategies by both
61 (10, 11). Phage resistance can evolve very rapidly in well-mixed liquid cultures of bacteria under phage
62 attack (2, 12, 13); for spatially structured environments, on the other hand, recent work has suggested that
63 selection for phage resistance can take on very different forms due to protection of phage-susceptible cells
64 in confined refugia (14–17). The generality of this prediction in realistic biofilm conditions is currently
65 unknown; here we leverage a custom biofilm-specific simulation framework and a microfluidics-based
66 experimental system to address this question.

67 Biofilms are characteristically heterogeneous, including steep gradients in nutrient availability,
68 waste product accumulation, oxygenation, and pH, among other factors (18, 19). Furthermore, biofilm
69 structure can impede the movement of solutes and particles that ordinarily would pose grave threats in
70 well-mixed liquid conditions. The extracellular matrix of *Pseudomonas aeruginosa*, for instance, can
71 block the diffusion of antibiotics such as tobramycin (20, 21). Biofilm matrix secreted by *Escherichia coli*
72 and *P. aeruginosa* can also alter phage movement (22, 23), and mucoid colony phenotypes, which
73 correlate with higher capsule or matrix secretion, rapidly evolve under lytic phage exposure in *E. coli* and
74 *P. fluorescens* (24, 25).

75 Beyond their deep importance to microbial natural history, phages' ability to rapidly destroy
76 susceptible populations makes them attractive as alternative antimicrobials (12, 26, 27). Optimizing
77 phages for this purpose, including an understanding of phage resistance evolution among host bacteria,
78 requires exploration of models and experiments that specifically capture the essential elements of biofilm
79 environments (28, 29). In particular, biofilm growth may have profound impacts on the relative advantages
80 and disadvantages of phage resistance, because the spatial structure within biofilms can potentially protect
81 susceptible cells from phage exposure (15, 17, 22, 23, 30, 31).

82 Here we use high resolution imaging of our experimental biofilm system to address this problem,
83 exploring the population dynamics of phages, sensitive bacteria, and resistant bacteria. Our observations
84 indicate that sensitive bacteria coexist at high densities alongside resistant bacteria because of the
85 protection afforded by spatial structure: the resistant bacteria block phage access to sensitive cells and
86 can even act as phage sinks. Computational studies developed in parallel to the experiments support this
87 interpretation and indicate that the protection of sensitive cells generalizes robustly to a wide range of

88 bacterial resistance mechanisms, fitness cost of phage resistance, baseline bacterial growth rates, and
89 diffusivity of phages inside and outside of the biofilm microenvironment.

90

91 **Results**

92 In biofilm environments, the population dynamics of bacteria and their lytic phages are driven by many
93 processes, including bacterial growth, cell-cell shoving, solute advection/diffusion, phage-host attachment
94 probabilities, phage lag time and burst size, and phage advection/diffusion, among others (9, 15). To study
95 these processes we expanded a simulation framework previously developed by our groups that captures
96 the biological and solute/particle transport processes inherent to biofilm communities (15) (SI Materials
97 and Methods; code available at <https://github.com/simbiofilm/simbiofilm> (32)). Our framework
98 implements the growth of up to hundreds of thousands of discrete bacteria and phages in explicit space; it
99 is custom-made for this application but falls within the family of biofilm simulation techniques that have
100 been highly successful in capturing the qualitative dynamics of natural systems (33–35). To begin a
101 simulation, cells are inoculated onto a solid surface at the bottom of a 2-D space with lateral periodic
102 boundary conditions. Growth-limiting nutrients diffuse from a bulk liquid layer at the top of the 2-D space
103 towards the biofilm front, where they can be depleted due to consumption by cells (Figure 1A). The
104 biofilm surface erodes in a height-dependent manner, reflecting the increase in shear rate with distance
105 from the surface (36). After a pre-set interval of biofilm growth, phages are introduced to the system in a
106 pulse at one location along the biofilm's upper surface (varying the timing or location of phage pulses had
107 little impact on the results, see Supplementary Information). In the simulations, phages can associate with
108 cells in the biofilm and initiate infections, or be released into the surrounding liquid, where they diffuse
109 for a full simulation iteration cycle prior to being swept out of the system by advection (Figure 1A). We
110 implemented phage diffusion by algorithmic rules that are described in detail in the SI Materials and
111 Methods.

112 To understand the population dynamics of phages in the presence of biofilms that contain both
113 susceptible and resistance bacterial strains, we constrained our simulations using experimentally measured
114 parameters for bacterial growth, phage replication, and nutrient diffusion (See Table S1), based on *E. coli*
115 and its lytic phage T7 (the same species used in our experiments, see below). We explored the impact of
116 factors that are likely to vary in natural environments where phage-biofilm interactions occur. The first is
117 nutrient availability, which controls overall biofilm expansion rate (37, 38). We also varied the initial
118 population ratio of susceptible to resistant host bacteria. In this way, we could test for the invasibility of

119 phage-resistant and phage-susceptible cells when rare. For example, if resistant cells always increase
120 (/decrease) in frequency regardless of their initial fraction, we can infer that they are being positively
121 (/negatively) selected. On the other hand, if they increase when initially rare but decrease when initially
122 common, then we can infer that resistant and susceptible cells will tend toward coexistence (39). We also
123 tested for the effect of variation in the fitness cost of phage resistance, variation in phage diffusivity,
124 variation in how phages were introduced to the biofilm surface, and whether phages were introduced at
125 earlier or later time points during biofilm growth (see Supplementary Information). Importantly we also
126 explored the impact, if any, of the mechanism of phage resistance.

127 Phage resistance can manifest in different ways; for example, in the case of *E. coli* and the lytic
128 phage T7, which attaches to LPS to initiate infection, the host can evolve resistance by modification or
129 partial loss of the LPS biosynthesis machinery, or by loss of thioredoxin A, which is co-opted and required
130 by T7 as a phage DNA polymerase processivity factor (40). In the case of LPS mutants, phages cannot
131 bind the cell surface, and thus phage-host encounters leave both phage and host intact. Mutants of *E. coli*
132 that have lost thioredoxin A, however, allow phage entry, but not replication, and thus cause an abortive
133 infection in which the host and the phage are both killed. In our experimental tests below, we use the
134 thioredoxin A mutant as our phage-resistant strain, and for correspondence we use for our simulations in
135 the main text a resistant mutant that both neutralizes phages and is neutralized when a phage attaches.
136 However we repeat all simulations for the scenario in which neither the host cell or phage is neutralized
137 by a contact event and phages are free to continue diffusing (such as for surface mutants), and for the
138 scenario in which the bacterial host is unaffected while the phage is neutralized by a contact event (such
139 as for CRISPR-Cas9 based immunity).

140

141 **Biofilms robustly facilitate coexistence of phage-resistant and -susceptible cells**

142 The full results of our parameter sweeps are shown in Figures S1 and S2, and for clarity we show a
143 representative sub-set of these results in Figure 1B, where the fitness cost (i.e. growth rate decrement) of
144 displaying phage resistance is a 5% reduction in maximum growth rate, and phages are moderately
145 impeded from diffusion in biofilms. On the scale of the whole biofilm simulation space, the overriding
146 pattern of our simulations was positive selection for phage resistant cells when they are initially rare, and
147 either neutral or negative selection for resistant cells when they are initially common (SI Figure S1; SI
148 Video S1 and Video S2). The only exceptions occur when phage mobility is extremely high, in which
149 case the system behaves as though it were a well-mixed culture and phage resistance is uniformly

150 positively selected (Figures S1); or when phage mobility is so severely constrained that viral particles
151 never have an opportunity to ‘find’ susceptible hosts by diffusion, in which case the phage-resistant and
152 phage-susceptible cells compete solely according to their growth rates (Figures S1). We observed the same
153 qualitative results when our simulations were implemented in 3-D space (SI Video S3 and Video S4). The
154 results were also the same regardless of the mode of resistance among the bacteria; the same trends were
155 upheld if the resistant strain caused abortive infections, if neither resistant hosts nor phages were
156 neutralized by mutual contact, or if phages alone were neutralized by contact with resistant hosts (Figure
157 S2).

158 The results broadly and robustly support the prediction of coexistence of phage-resistant and
159 phage-susceptible cells in biofilm environments. We observed the same qualitative pattern as shown in
160 Figure 1B when we varied the biofilm size at which phages were introduced, and there was similarly little
161 effect if phages were introduced at a single point or evenly along the entire biofilm surface (Figure S3).
162 The strength of negative frequency-dependent selection, and the predicted stable frequencies of resistance
163 and susceptible cells, are tuned by phage mobility and the cost of phage resistance (15), but the overall
164 qualitative pattern of predicted coexistence is highly robust to parameter changes (Figure S1) (39, 41–43).
165 We next looked for the details of this negative frequency-dependence: why do phage-resistant cells fare
166 well when rare, but fare poorly when common?

167 ***Clearance of susceptible cells when they are common*** – When phage-susceptible cells start in the
168 majority within a biofilm, the few resistant cells initially in the population are concentrated into small
169 isolated groups. As a result, when phages enter the system, they have ready access to susceptible hosts
170 that occupy the majority of space, and the propagating infection eliminates most or all of the susceptible
171 population. After this clearance event, the few remaining phage-resistant cells have an abundance of open
172 space to occupy as they continue to grow with reduced competition for nutrient sources in the surrounding
173 medium (Figure 2A,B). Unless the cost of phage resistance is very high (Figure S1), resistant cells tend
174 not to reach fixation due to small pockets of susceptible cells that are protected from phage exposure by
175 neighboring resistant cells (Figure 2B). This latter effect is strengthened if resistant cells are initially
176 abundant, as detailed below.

177 ***Phage sequestering by resistant cells when they are common*** – When phage-resistant cells are
178 initially common, phage-susceptible cell clusters are isolated among larger groups of resistant cells. If
179 phage diffusion is even moderately impeded by the presence of biofilm, then susceptible cells gain
180 protection from phages. This occurs because phages become trapped on the periphery of clusters of

181 resistant cells, and because phages released into the liquid phase are often blocked from long-range
182 movement by groups of resistant cells in their path. The lower the frequency of susceptible cells in the
183 initial inoculum, the stronger the effect of these spatial phage protection mechanisms. In this scenario, if
184 there is no cost to resistance, then susceptible and resistant cells compete neutrally. If there is a fitness
185 cost to resistance, then susceptible cells have an intrinsic growth rate advantage, and they increase in
186 frequency if they are initially rare (Figure 2A,C).

187 188 **Experimental model of phage resistance population dynamics**

189 Our simulation results strongly support the prediction for coexistence of phage-susceptible and phage-
190 resistant cells in biofilm environments, nearly regardless of variation in any major features of the system.
191 Here we set out to test this prediction using an experimental model of biofilm growth under lytic phage
192 attack. Biofilms of *E. coli* were cultivated in microfluidic devices, including co-cultures of wild type
193 AR3110 (WT), which is T7-susceptible, and an isogenic strain harboring a clean deletion of *trxA*, which
194 does not support phage replication (see Materials and Methods). The $\Delta trxA$ mutant lacks thioredoxin A,
195 which is an essential DNA processivity factor for the lytic phage T7. This deletion mutant therefore causes
196 an abortive infection in which phage attachment occurs and the host is killed, but the phage is not able to
197 replicate or lyse the host (40). We chose the $\Delta trxA$ mutant as representative of phage-resistant variants
198 because it does not support phage propagation but is able to form biofilms normally. Almost all other
199 mutations conferring T7 resistance are in the LPS assembly machinery, and our pilot experiments
200 indicated that these mutant classes are severely defective for biofilm formation, and so do not allow the
201 experiments described below to be performed. This biofilm defect is a notable fitness cost of LPS-
202 modification-dependent phage resistance, but in order to test our predictions we required a T7-resistant
203 mutant capable of biofilm formation and thus focus on the $\Delta trxA$ background for the remainder of the
204 paper. Growth curves in shaken liquid media identical to that used for biofilm experiments indicated that
205 the phage-resistant $\Delta trxA$ mutant has a growth rate cost of 7.9% +/- 0.69% (Figure S4)

206 The *E. coli* experimental biofilms were cultivated in microfluidic devices composed of a chamber
207 molded into PDMS, which was then bonded to a glass coverslip for imaging on an inverted confocal
208 microscope. Prior work has shown that even biofilms of phage-susceptible WT *E. coli* AR3110 can protect
209 themselves from phages after ~60 h of growth, when they begin to produce a curli amyloid fiber mesh
210 that blocks phage diffusion (23). Here biofilms of WT and $\Delta trxA$ mutant were cultivated for only 48 hours
211 prior to phage exposure, such that no curli-mediated phage protection could occur during the initial phage

212 exposure. In different runs of the experiment, mimicking our simulation approach, we inoculated the glass
213 bottom of flow devices with varying ratios of phage-susceptible and phage-resistant bacterial cells.
214 Analogous to the simulations, we allowed biofilms to grow undisturbed for 48 hours and then subjected
215 them to a pulse of high-density phage suspensions (Figure S5; Materials and Methods). Biofilm
216 populations were then imaged by confocal microscopy at regular intervals for 2 days. For each imaging
217 session, the entire biofilm volume was captured in successive optical sections.

218 We found that when phage-resistant cells were initially rare, susceptible cells were killed off by
219 phage exposure and mostly cleared out of the chambers, opening new space into which resistant cells
220 could grow for the remainder of the experiment (Figure 3A,B). As in our simulations, resistant cells often
221 did not reach fixation, as small clusters of susceptible cells remained. On the other hand, when phage-
222 resistant cells were initially common (~60% of the population, or more), the relative fraction of resistant
223 and susceptible host bacteria did not substantially change following phage treatment (Figure 3A,C). We
224 did not observe localized cycling of resistant and susceptible cells, as one might predict in closed and
225 shaken liquid culture conditions, most likely because phages were either sequestered locally within
226 clusters of resistant cells (Figure 4), or advected out of the system by ongoing fluid flow in our
227 microfluidic devices.

228 Our experimental results thus displayed a good qualitative match to our models. The spatial
229 patterns underlying these outcomes were the same as those observed in our simulations, including a
230 clearance of susceptible cells when resistant cells are initially rare. In this condition, susceptible cells are
231 exposed to phages; the remaining resistant cell clusters then have ample room to multiply (Figure 3B).
232 Our experiments also confirmed that susceptible cells are protected when they are initially rare: when
233 resistant cells are common, they often sequester phages away from susceptible cells, which then remain
234 near their initial frequency in the population (Figure 3C). To further test this inference, we introduced
235 fluorescently labelled T7 phages to biofilms initiated with a majority of resistant bacteria, and directly
236 observed that these phages immobilized in regions of the biofilm occupied purely by resistant cells (Figure
237 4, additional replicas in Figure S6).

238

239 **Discussion**

240 Our results provide a foundation for understanding how decreased phage mobility and sequestration to
241 resistant hosts within biofilms determine the population dynamics of phage resistance. Using simulations
242 with extensive parameter sweeps, we found a dominating trend toward negative frequency-dependent

243 selection for phage resistance that is remarkably robust to parameter changes. This outcome is matched
244 by our microfluidic model of biofilm formation visualized at single cell resolution, and it reinforces and
245 generalizes predictions from more abstracted models in the literature (14, 16, 29).

246 The origins of frequency-dependent selection are tied to the cell movement constraints and
247 competition for space in biofilms. When phage-resistant bacteria are initially rare, introduced phages have
248 open access to susceptible hosts, which are mostly killed, leaving empty space for the residual resistant
249 cell clusters to occupy. On the other hand, when phage-resistant bacteria are initially common, they create
250 barriers between phages and clusters of susceptible cells. So long as there is impeded diffusion of phages
251 through the biofilm volume, this spatial arrangement provides protection to susceptible cells, whose
252 population frequency can then drift or increase significantly depending on the fitness costs of phage
253 resistance. On the basis of our parameter sensitivity analyses, we infer that this pattern is an inevitable
254 consequence of the spatial constraints inherent to biofilm communities.

255 We tested these outcomes experimentally using microfluidic culture and confocal microscopy of
256 mixed *E. coli* biofilms containing resistant and susceptible hosts; these trials gave an excellent qualitative
257 match to the simulations, and we could document both the clearance and phage sequestration effects,
258 depending, as anticipated from simulations, on the initial fractions of resistant and susceptible bacterial
259 cells. Because LPS mutants of *E. coli* appear to be severely impaired for biofilm formation, we were only
260 able to experimentally test the case in which abortive infection is the resistance mechanism. In this manner
261 phages are limited in their diffusion not only because of barriers of resistant cells, but also because of
262 sorptive scavenging; that is, they are sequestered by resistant cells, and both the host and phage are
263 neutralized by the encounter (16, 44–48). We emphasize, however, that our simulations very strongly
264 suggest that even in the event that neither host nor phage is neutralized by a mutual encounter and phages
265 are free to continue diffusing, such as when a mutant gains phage resistance via loss of the cell surface
266 phage receptor, the same pattern of negative frequency-dependent selection for resistance will be upheld
267 in the vast majority of conditions.

268 Our results also draw an analogy between phage ‘epidemics’ on the sub-millimeter scale of
269 biofilms and the process of herd immunity studied for decades at much larger spatial scales in populations
270 of plants and animals (49–51). When enough of the population is resistant, a spreading pathogen is no
271 longer able to establish sufficient infections to amplify itself, and the susceptible portion of the population
272 is protected (49). These observations in turn have several general implications. We anticipate that the arms
273 race of phage attack and host defense can have a very different landscape in biofilms compared with

274 planktonic populations (2, 5, 7, 14, 52). A rich history of research has shown that phages can rapidly
275 eliminate susceptible host cell populations in mixed liquid culture, leading to strong selection for phage
276 resistance (2–4, 53). In biofilms, by contrast, our results predict widespread and easily maintained
277 polymorphism in phage resistance ability. This kind of standing variation can arise due to minority
278 advantage (i.e., kill-the-winner) mechanisms (54–57), in which phages or other parasites are selected to
279 target the most abundant constituent strains of a population.

280 The mechanism we describe here is distinct from kill-the-winner based selection, but
281 complementary: susceptible cells in the minority are unlikely to be exposed to phages in the first place, as
282 they are shielded by resistant cells blocking phage diffusion. The arms race between phages and host
283 bacteria, therefore, is likely to take different evolutionary trajectories that move at slower speeds than
284 those typically observed in liquid culture. This outcome echoes results observed in the early phage-host
285 coevolution literature, where it found that for bacteria that form ‘wall populations’ on the inside of shaken
286 liquid culture tubes, phage-susceptible bacteria survive at much higher rates than in the well-mixed
287 planktonic phase (58). These wall populations are now known as biofilms, and here we have directly
288 visualized the spatial protection process that allows susceptible cells to survive where otherwise they
289 would not. The results obtained here also make concrete on the microscopic scale how variable access of
290 phages to susceptible hosts shifts populations to steady states in which phage-resistant and phage-
291 susceptible bacteria should robustly coexist (5, 14).

292 Our observations also bear on the efficacy of phage therapies, for which one of the most promising
293 potential benefits is selective elimination of target pathogens from a community of otherwise commensal
294 or beneficial microbes (12, 27, 56, 59, 60). This is a particularly compelling advantage relative to broad-
295 spectrum antibiotics that can kill off not just the target pathogen but also many other members of a
296 patient’s microbiota, sometimes with severe side effects (61). Our work suggests that while it might be
297 possible to completely eliminate target bacteria with lytic phages from a mixed population, the success of
298 this approach depends heavily on the community composition and spatial structure. Phage-susceptible
299 cells can be much harder to target and can coexist with resistant cells, or presumably cells of other species
300 that phage cannot target, due to the protective effects of phage sequestration and diffusional blocking.
301 Successful phage treatment will likely depend on disruption of the biofilm architecture to ensure exposure
302 of target bacteria to the therapeutic. It should be noted, however, that our work here only examines two
303 strains of the same species, and whether these conclusions apply to multi-species consortia (62), whose
304 biofilm architectures can differ substantially, is an important topic for further work.

305 The models developed here do not address the possibility of refuges created by quiescent bacteria
306 in the basal layers of biofilms where nutrients have been depleted (14). This did not appear to be an
307 important feature of our experimental biofilms, which agreed well with simulation predictions. However,
308 quiescent cells could potentially be significant in other conditions, especially for cell groups that
309 accumulate thicker mats with large, nutrient-starved populations in their interior. We also do not
310 implement ongoing mutations in the different bacterial and phage strains residing in biofilms, using
311 instead strains that are fixed in either the phage-susceptible or -resistant state to examine short term
312 population dynamics. Lastly, and importantly, we omitted from our simulations and experiments the
313 possibility of temperate phage infections, in which the phage genome is inserted to the chromosome of
314 the host organism, emerging to replicate and produce new phages when the host is under duress.
315 Temperate phages present a wide diversity of potential outcomes, especially considering that they can
316 impart new phenotypes to their bacterial hosts. Tackling the challenge, both theoretically and
317 experimentally, of how temperate phages enter, alter, and evolve within multispecies microbial
318 communities is an important area for future work.

319

320 **Author Contributions**

321 CDN conceived and supervised the project; CDN and VB designed simulations and experiments. MS
322 developed the simulation framework and performed simulation data collection. MCB performed
323 experiments and image processing of microscopy data. MKS, MCB, BK, KD, VB, and CDN analyzed
324 and interpreted data. MKS, MCB, BK, KD, VB, and CDN wrote the paper.

325

326

327

328 **Acknowledgements**

329 We are grateful to Will Harcombe, Wolfram Möbius, Ben Wucher, Swetha Kasetty, and Sara Mitri for
330 comments on earlier versions of the manuscript. Input from Jim Bull was invaluable in completing the
331 paper. MCB is supported by a GANN Fellowship from Dartmouth College. KD is supported by the
332 European Research Council (StG-716734), the Deutsche Forschungsgemeinschaft (SFB 987), and the
333 Behrens-Weise-Foundation. VB is supported by NSF ABI 1458347 and a UMass President Science and
334 Technology award. CDN is supported by the National Science Foundation MCB 1817342, a Burke Award

335 from Dartmouth College, a pilot award from the Cystic Fibrosis Foundation (STANTO15RO), NIH grant
336 P30-DK117469, and NIH grant P20-GM113132 to the Dartmouth BioMT COBRE.

337

338 **References**

- 339 1. Susskind MM, Botstein D (1978) Molecular genetics of bacteriophage P22. *Microbiol Rev*
340 42(2):385–413.
- 341 2. Koskella B, Brockhurst MA (2014) Bacteria–phage coevolution as a driver of ecological and
342 evolutionary processes in microbial communities. *Fems Microbiol Rev* 38(5):916–931.
- 343 3. Lenski RE, Levin BR (1985) Constraints on the coevolution of bacteria and virulent phage: a
344 model, some experiments, and predictions for natural communities. *Am Nat*:585–602.
- 345 4. Chao L, Levin BR, Stewart FM (1977) A Complex Community in a Simple Habitat: An
346 Experimental Study with Bacteria and Phage. *Ecology* 58(2):369–378.
- 347 5. Brockhurst MA, Buckling A, Rainey PB (2006) Spatial heterogeneity and the stability of host-
348 parasite coexistence. *J Evol Biol* 19(2):374–379.
- 349 6. Harrison E, Laine A-L, Hietala M, Brockhurst MA (2013) Rapidly fluctuating environments
350 constrain coevolutionary arms races by impeding selective sweeps. *Proc R Soc B*
351 280(1764):20130937.
- 352 7. Brockhurst MA, Buckling A, Rainey PB (2005) The effect of a bacteriophage on diversification
353 of the opportunistic bacterial pathogen, *Pseudomonas aeruginosa*. *Proc R Soc B* 272(1570):1385–
354 1391.
- 355 8. Abedon ST (2008) Bacteriophage Ecology: Population Growth, Evolution, and Impact of
356 Bacterial Viruses.
- 357 9. Abedon ST (2011) *Bacteriophages and Biofilms* (Nova Science).
- 358 10. Labrie SJ, Samson JE, Moineau S (2010) Bacteriophage resistance mechanisms. *Nat Rev Micro*
359 8(5):317–327.
- 360 11. Samson JE, Magadan AH, Sabri M, Moineau S (2013) Revenge of the phages: defeating bacterial
361 defences. *Nat Rev Micro* 11(10):675–687.
- 362 12. Levin BR, Bull JJ (2004) Population and evolutionary dynamics of phage therapy. *Nat Rev*
363 *Microbiol* 2(2):166–173.
- 364 13. Weitz JS, et al. (2013) Phage–bacteria infection networks. *Trends Microbiol* 21(2):82–91.
- 365 14. Heilmann S, Sneppen K, Krishna S (2012) Coexistence of phage and bacteria on the boundary of
366 self-organized refuges. *Proc Natl Acad Sci U S A* 109(31):12828–12833.
- 367 15. Simmons M, Drescher K, Nadell CD, Bucci V (2017) Phage mobility is a core determinant of
368 phage–bacteria coexistence in biofilms. *Isme J* 12:531–543.
- 369 16. Bull JJ, et al. (2018) Phage-Bacterial Dynamics with Spatial Structure: Self Organization around
370 Phage Sinks Can Promote Increased Cell Densities. *Antibiotics* 7(1):8.
- 371 17. Eriksen RS, Svenningsen SL, Sneppen K, Mitarai N (2018) A growing microcolony can survive
372 and support persistent propagation of virulent phages. *Proc Natl Acad Sci U S A* 115(2):337–342.
- 373 18. Stewart PS, Franklin MJ (2008) Physiological heterogeneity in biofilms. *Nat Rev Microbiol*
374 6(3):199–210.
- 375 19. Stewart PS (2012) Mini-review: Convection around biofilms. *Biofouling* 28(2):187–198.
- 376 20. Mah T-FC, O’Toole GA (2001) Mechanisms of biofilm resistance to antimicrobial agents. *Trends*
377 *Microbiol* 9(1):34–39.
- 378 21. Tseng BS, et al. (2013) The extracellular matrix protects *Pseudomonas aeruginosa* biofilms by
379 limiting the penetration of tobramycin. *Environ Microbiol* 15(10):2865–2878.

- 380 22. Darch SE, et al. (2017) Phage Inhibit Pathogen Dissemination by Targeting Bacterial Migrants in
381 a Chronic Infection Model. *MBio* 8(2):e00240-17.
- 382 23. Vidakovic L, Singh PK, Hartmann R, Nadell CD, Drescher K (2018) Dynamic biofilm
383 architecture confers individual and collective mechanisms of viral protection. *Nat Microbiol*
384 3:26–31.
- 385 24. Chaudhry WN, et al. (2019) Mucoidy, a general mechanism for maintaining lytic phage in
386 populations of bacteria. *bioRxiv* 775056.
- 387 25. Scanlan PD, Buckling A (2012) Co-evolution with lytic phage selects for the mucoid phenotype
388 of *Pseudomonas fluorescens* SBW25. *ISME J* 6(6):1148–1158.
- 389 26. Abedon ST, Thomas-Abedon C (2010) Phage Therapy Pharmacology. *Curr Pharm Biotechnol*
390 11(1):28–47.
- 391 27. Chan BK, Abedon ST (2012) Phage Therapy Pharmacology: Phage Cocktails. *Advances in*
392 *Applied Microbiology, Vol 78*, eds Laskin AI, Sariaslani S, Gadd GM, pp 1–23.
- 393 28. Azeredo J, Sutherland IW (2008) The use of phages for the removal of infectious biofilms. *Curr*
394 *Pharm Biotechnol* 9(4):261–266.
- 395 29. Sutherland IW, Hughes KA, Skillman LC, Tait K (2004) The interaction of phage and biofilms.
396 *Fems Microbiol Lett* 232(1):1–6.
- 397 30. Chaudhry WN, et al. (2018) Leaky resistance and the conditions for the existence of lytic
398 bacteriophage. *PLOS Biol* 16(8):e2005971.
- 399 31. Bull JJ, Vegge CS, Schmerer M, Chaudhry WN, Levin BR (2014) Phenotypic Resistance and the
400 Dynamics of Bacterial Escape from Phage Control. *PLoS One* 9(4):e94690.
- 401 32. Simmons M, Bucci V, Nadell C (2019) SimBiofilm: A framework for individual-based biofilm
402 modeling with bacteriophage infection. Available at: <https://github.com/simbiofilm/simbiofilm>.
- 403 33. Nadell CD, Drescher K, Foster KR (2016) Spatial structure, cooperation, and competition in
404 bacterial biofilms. *Nat Rev Microbiol* 14:589–600.
- 405 34. Picioreanu C, Xavier JB, van Loosdrecht MCM (2005) Advances in mathematical modeling of
406 biofilm structure. *Biofilms* 1(04):337–349.
- 407 35. Xavier JB, Picioreanu C, van Loosdrecht MCM (2005) A framework for multidimensional
408 modelling of activity and structure of multispecies biofilms. *Environ Microbiol* 7(8):1085–1103.
- 409 36. Xavier JB, Picioreanu C, van Loosdrecht M (2005) A general description of detachment for
410 multidimensional modelling of biofilms. *Biotechnol Bioeng* 91(6):651–669.
- 411 37. Picioreanu C, van Loosdrecht MCM, Heijnen JJ (1998) A new combined differential-discrete
412 cellular automaton approach for biofilm modeling: Application for growth in gel beads.
413 *Biotechnol Bioeng* 57(6):718–731.
- 414 38. Nadell CD, et al. (2013) Cutting through the complexity of cell collectives. *Proc R Soc B*
415 280(1755):20122770.
- 416 39. Siepielski AM, McPeck MA (2010) On the evidence for species coexistence: a critique of the
417 coexistence program. *Ecology* 91(11):3153–64.
- 418 40. Qimron U, Marintcheva B, Tabor S, Richardson CC (2006) Genomewide screens for *Escherichia*
419 *coli* genes affecting growth of T7 bacteriophage. *Proc Natl Acad Sci* 103(50):19039–19044.
- 420 41. MacArthur R (1972) *Geographical Ecology* (Princeton University Press, Princeton, NJ).
- 421 42. Levin SA (1970) Community Equilibria and Stability, and an Extension of the Competitive
422 Exclusion Principle. *Am Nat* 104(939):413–423.
- 423 43. Chesson P (2000) Mechanisms of Maintenance of Species Diversity. *Annu Rev Ecol Syst*
424 31(1):343–366.
- 425 44. Yin J, McCaskill J (1992) Replication of viruses in a growing plaque: a reaction-diffusion model.

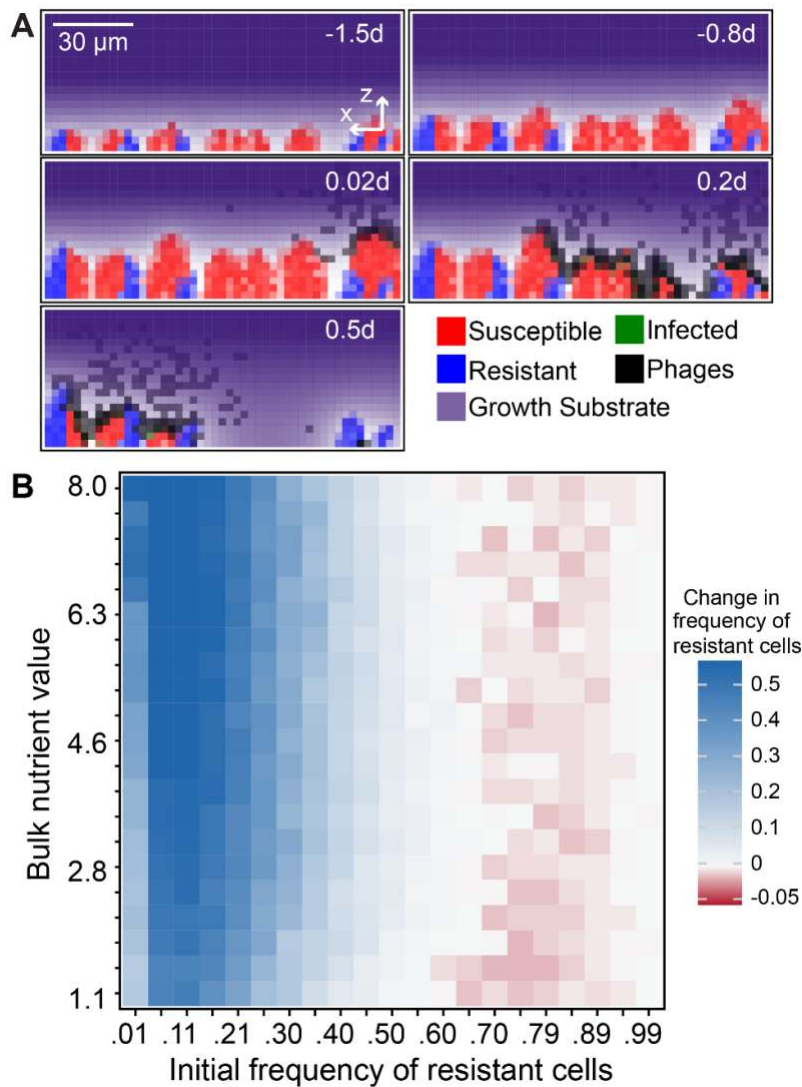
- 426 *Biophys J* 61:1540–1549.
- 427 45. Hewson I, Fuhrman J (2003) Vibriobenthos production and virioplankton sorptive scavenging.
428 *Microb Ecol* 46:337–347.
- 429 46. Rabinovitch A, Aviram I, Zaritsky A (2003) Bacterial debris - an ecological mechanism for
430 coexistence of bacteria and their viruses. *J Theor Biol* 224:377–383.
- 431 47. Abedon ST (2017) Phage “delay” toward enhancing bacterial escape from biofilms: a more
432 comprehensive way of viewing resistance to bacteriophages. *AIMS Microbiol* 3(2):186–226.
- 433 48. Abedon ST (2016) Bacteriophage exploitation of bacterial biofilms: phage preference for less
434 mature targets? *Fems Microbiol Lett* 363(3):fnv246.
- 435 49. Metcalf CJE, Ferrari M, Graham AL, Grenfell BT (2015) Understanding Herd Immunity. *Trends*
436 *Immunol* 36(12):753–755.
- 437 50. Levin SA, Durrett R (1996) From individuals to epidemics. *Philos Trans R Soc B Biol Sci*
438 351(1347):1615–1621.
- 439 51. Levin SA (1992) The Problem of Pattern and Scale in Ecology: The Robert H. MacArthur Award
440 Lecture. *Ecology* 73(6):1943–1967.
- 441 52. Davies E V, et al. (2016) Temperate phages both mediate and drive adaptive evolution in
442 pathogen biofilms. *Proc Natl Acad Sci* 113(29):8266–8271.
- 443 53. Levin BR, Stewart FM, Chao L (1977) Resource-Limited Growth, Competition, and Predation: A
444 Model and Experimental Studies with Bacteria and Bacteriophage. *Am Nat* 111(977):3–24.
- 445 54. Díaz-Muñoz SL, Koskella B (2014) Bacteria-phage interactions in natural environments. *Adv*
446 *Appl Microbiol* 89(135):10.1016.
- 447 55. Koskella B, Thompson JN, Preston GM, Buckling A (2011) Local biotic environment shapes the
448 spatial scale of bacteriophage adaptation to bacteria. *Am Nat* 177(4):440–451.
- 449 56. Koskella B, Meaden S, Koskella B, Meaden S (2013) Understanding Bacteriophage Specificity in
450 Natural Microbial Communities. *Viruses* 5(3):806–823.
- 451 57. Kunin V, et al. (2008) A bacterial metapopulation adapts locally to phage predation despite global
452 dispersal. *Genome Res* 18(2):293–7.
- 453 58. Schrag SJ, Mittler JE (1996) Host-Parasite Coexistence: The Role of Spatial Refuges in
454 Stabilizing Bacteria-Phage Interactions. *Am Nat* 148(2):348–377.
- 455 59. Levin BR, Bull JJ (1996) Phage therapy revisited: The population biology of a bacterial infection
456 and its treatment with bacteriophage and antibiotics. *Am Nat* 147(6):881–898.
- 457 60. Sillankorva S, Neubauer P, Azeredo J (2010) Phage control of dual species biofilms of
458 *Pseudomonas fluorescens* and *Staphylococcus lentus*. *Biofouling* 26(5):567–575.
- 459 61. Buffie CG, et al. (2012) Profound Alterations of Intestinal Microbiota following a Single Dose of
460 Clindamycin Results in Sustained Susceptibility to *Clostridium difficile*-Induced Colitis. *Infect*
461 *Immun* 80(1):62–73.
- 462 62. Harcombe WR, Bull JJ (2005) Impact of phages on two-species bacterial communities. *Appl*
463 *Environ Microbiol* 71(9):5254–9.
- 464 63. Guyer JE, Wheeler D, Warren JA (2009) FiPy: Partial Differential Equations with Python.
465 *Comput Sci Eng* 11(3):6–15.
- 466 64. Lardon LA, et al. (2011) iDynoMiCS: next-generation individual-based modelling of biofilms.
467 *Environ Microbiol* 13(9):2416–2434.
- 468 65. Bucci V, Hoover S, Hellweger FL (2012) Modeling Adaptive Mutation of Enteric Bacteria in
469 Surface Water Using Agent-Based Methods. *Water, Air, Soil Pollut* 223(5):2035–2049.
- 470 66. Hellweger FL, Bucci V (2009) A bunch of tiny individuals-Individual-based modeling for
471 microbes. *Ecol Modell* 220(1):8–22.

- 472 67. Bucci V, Nadell CD, Xavier JB (2011) The evolution of bacteriocin production in bacterial
473 biofilms. *Am Nat* 178(6):E162–E173.
- 474 68. Nadell CD, Foster KR, Xavier JB (2010) Emergence of spatial structure in cell groups and the
475 evolution of cooperation. *PLoS Comput Biol* 6(3):e1000716.
- 476 69. Hallatschek O, Hersen P, Ramanathan S, Nelson DR (2007) Genetic drift at expanding frontiers
477 promotes gene segregation. *Proc Natl Acad Sci USA* 104(50):19926–19930.
- 478 70. Datsenko KA, Wanner BL (2000) One-step inactivation of chromosomal genes in *Escherichia*
479 *coli* K-12 using PCR products. *Proc Natl Acad Sci U S A* 97(12):6640–5.
- 480 71. Weibel DB, DiLuzio WR, Whitesides GM (2007) Microfabrication meets microbiology. *Nat Rev*
481 *Microbiol* 5(3):209–218.
- 482 72. Sia SK, Whitesides GM (2003) Microfluidic devices fabricated in poly(dimethylsiloxane) for
483 biological studies. *Electrophoresis* 24:3563–3576.
- 484 73. Bonilla N, et al. (2016) Phage on tap—a quick and efficient protocol for the preparation of
485 bacteriophage laboratory stocks. *PeerJ* 4:e2261.
- 486 74. Drescher K, Nadell CD, Stone HA, Wingreen NS, Bassler BL (2014) Solutions to the Public
487 Goods Dilemma in Bacterial Biofilms. *Curr Biol* 24(1):50–55.
- 488 75. Nadell CD, Drescher K, Wingreen NS, Bassler BL (2015) Extracellular matrix structure governs
489 invasion resistance in bacterial biofilms. *ISME J* 9:1700–1709.
- 490 76. McCarty PL (2012) *Environmental biotechnology: principles and applications* (Tata McGraw-
491 Hill Education).
- 492 77. Stewart P (2003) Diffusion in Biofilms. *J Bacteriol* 185(5):1485–1491.
- 493 78. Henze M, Grady Jr CPL, Gujer W, Marais GVR, Matsuo T (1987) Activated sludge model no. 1:
494 IAWPRC scientific and technical report no. 1. *IAWPRC, London*.
- 495 79. Henze M, et al. (1999) Activated Sludge Model No.2d, ASM2d. *Water Sci Technol* 39(1):165–
496 182.
- 497 80. Oliveira CS, et al. (2009) Determination of kinetic and stoichiometric parameters of *Pseudomonas*
498 *putida* F1 by chemostat and in situ pulse respirometry. *Chem Prod Process Model* 4(2).
- 499 81. Loferer-Krößbacher M, Klima J, Psenner R (1998) Determination of Bacterial Cell Dry Mass by
500 Transmission Electron Microscopy and Densitometric Image Analysis. *Appl Environ Microbiol*
501 64(2):688–694.
- 502 82. Lapidou CS, Rittmann BE (2002) Non-steady state modeling of extracellular polymeric
503 substances, soluble microbial products, and active and inert biomass. *Water Res* 36(8):1983–
504 1992.
- 505 83. Narang A, Konopka A, Ramkrishna D (1997) New patterns of mixed-substrate utilization during
506 batch growth of *Escherichia coli* K12. *Biotechnol Bioeng* 55(5):747–757.
- 507 84. Beg QK, et al. (2007) Intracellular crowding defines the mode and sequence of substrate uptake
508 by *Escherichia coli* and constrains its metabolic activity. *Proc Natl Acad Sci* 104(31):12663–
509 12668.
- 510 85. Trojanowicz K, Styka W, Baczynski T (2009) Experimental determination of kinetic parameters
511 for heterotrophic microorganisms in biofilm under petrochemical wastewater conditions. *Polish J*
512 *Environ Stud* 18(5).
- 513 86. Lapidou CS, Rittmann BE (2004) Modeling the development of biofilm density including active
514 bacteria, inert biomass, and extracellular polymeric substances. *Water Res* 38(14–15):3349–3361.
- 515 87. Esquivel-Rios I, et al. (2014) A microrespirometric method for the determination of
516 stoichiometric and kinetic parameters of heterotrophic and autotrophic cultures. *Biochem Eng J*
517 83:70–78.

- 518 88. Abedon ST (2009) Kinetics of Phage-Mediated Biocontrol of Bacteria. *Foodborne Pathog Dis*
519 6(7):807–815.
520

521
522

Figures



523

524

525

526

527

528

529

530

531

532

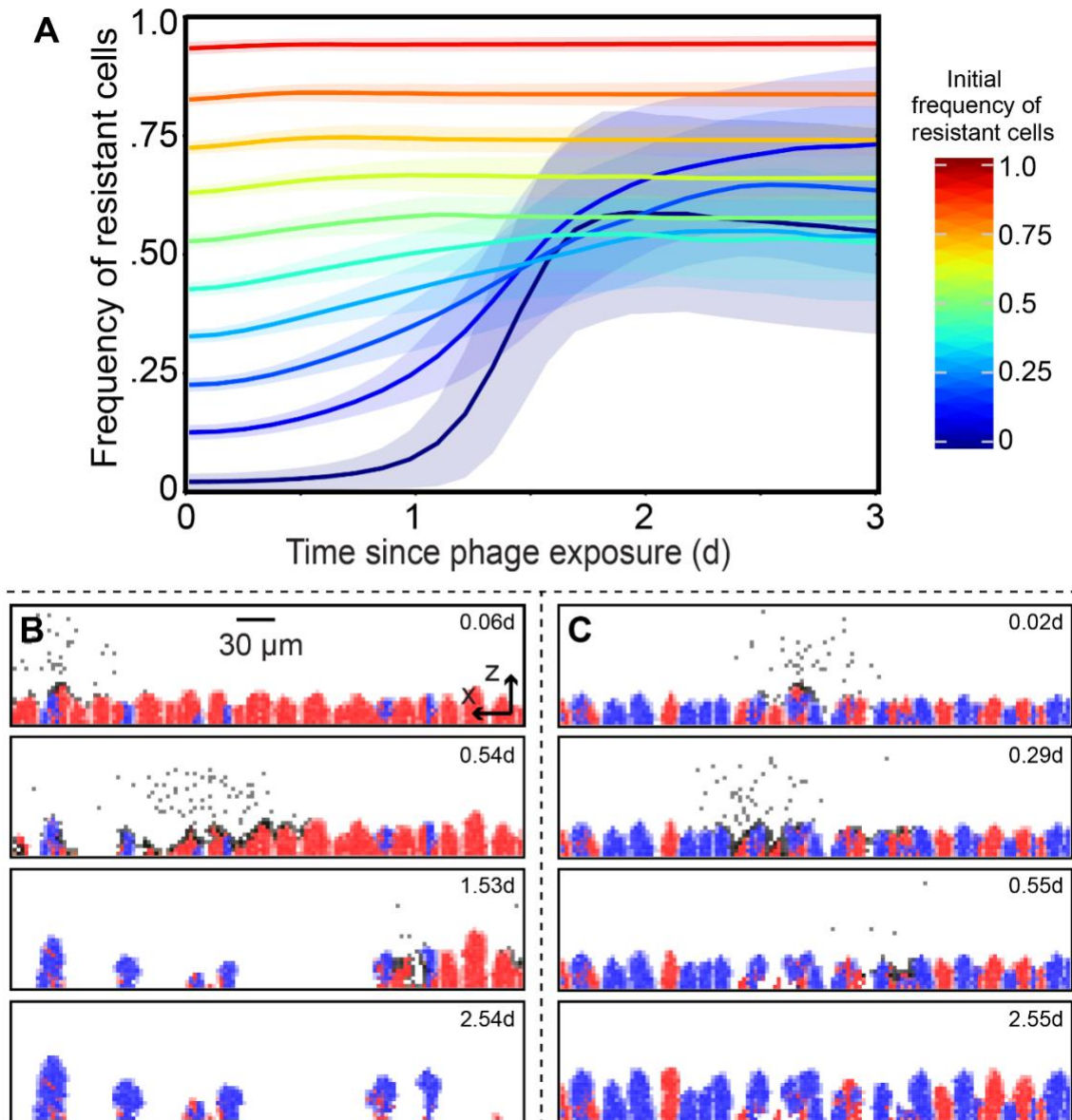
533

534

535

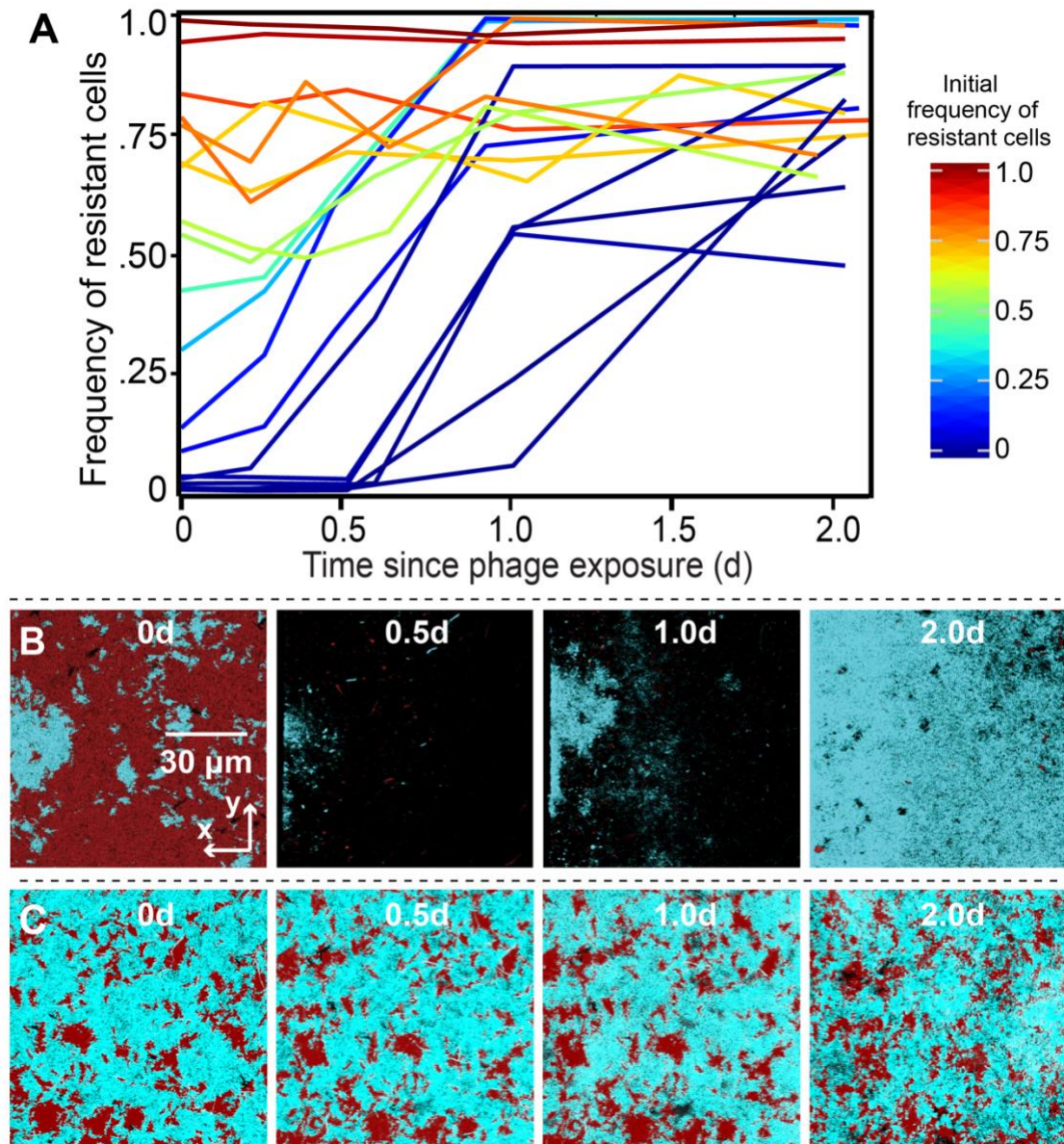
536

Figure 1. Simulated outcomes of phages exposed to biofilms composed of resistant and susceptible cells. (A) Example time series in which biofilms of phage-resistant and phage-susceptible cells are allowed to reach a critical height before introduction of phages at one location along the biofilm surface (varying the initial biofilm height and phage introduction procedure are explored in Figure S3). Phages can absorb to resistant cells but cannot amplify within them, and phages that have departed the biofilm - if they do not re-infect within the next time step - are assumed to be removed by fluid advection. (B) Summary heatmap of the effect of biofilm structure on selection for phage resistance. In the heatmap, simulation outcomes are shown for varying degrees of nutrient availability (which controls the baseline host growth rate) and initial resistant strain frequency. Here both phage mobility and removal rate from the liquid phase are intermediate, and the bacterial fitness cost of phage resistance is 5% of the maximum growth rate (see Figure S1 for extensive exploration of these factors). Resistant cells increase in frequency when initially uncommon (blue squares in heatmap), but when they are initially common, their relative abundance either stays the same (white squares) or decreases (red squares).



537
538

539 **Figure 2. Simulated population dynamics of phage-resistant and susceptible bacteria within biofilms.** These
540 dynamics underlie the competition outcomes in Figure 1. (A) The frequency of resistant cells is shown in traces
541 colored according to their initial frequency, with the standard deviation across all replicate runs as transparent blue
542 regions around each trace ($n = 90$ -100 replicate simulations per trace). (B) When resistant cells are initially a
543 minority, susceptible cells are exposed to phages and largely killed off, allowing resistant cells to re-seed the
544 population and markedly increase in relative abundance relative to the strain ratio prior to phage exposure. (C)
545 When resistant cells are initially more common, and phages cannot diffuse freely through the biofilm, susceptible
546 cells are spatially protected from phage exposure because phages are sequestered in clusters of resistant cells.



547

548

549

550

551

552

553

554

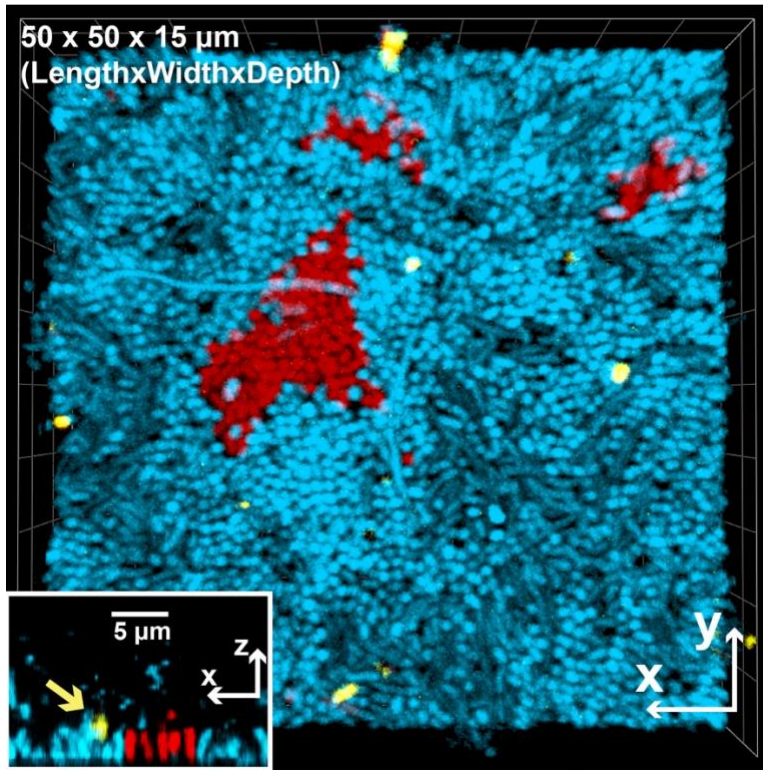
555

556

557

558

Figure 3. Experimental test of model predictions for phage-biofilm coexistence. Biofilms containing mixtures of phage T7-susceptible AR3110 *E. coli* and a phage T7-resistant mutant carrying a deletion of *trxA* were grown for 48 hours before administering a pulse of phages to the two-strain biofilm population. The frequency of resistant cells is shown in traces colored according to their initial frequency, where each trace is an independent run of the experiment. (A) Population dynamics traces showing the frequency of phage-resistant *E. coli* as a function of its initial population frequency. Each trace is a single replicate of the experiment, with varying initial ratios of the two strains as in our simulations (B, C) Time series of phage-resistant (blue) and phage-susceptible cells (red) following a pulse of phages into the chambers. Panels from left to right show biofilms at ~ 0, 0.5, 1, and 2 days after phage exposure. Each image is an x-y optical section from a stack of images covering the whole biofilm volume, taken by confocal microscopy.



559
560
561
562
563
564
565
566
567
568
569
570

Figure 4. Experimental demonstration of phage sequestration within clusters of phage-resistant bacteria (blue) in a mixed-strain biofilm with phage-susceptible bacteria (red). Purified phages stained with Alexafluor-633 (shown in yellow) were added to 48 h biofilms in which resistant cells were inoculated as 95% of the founding population. The central image is a top-down view of a 3-D rendering measuring 50 μ m x 50 μ m x 15 μ m [L x W x D]. The inset image is a 2-D projection of a vertical slice through a 3-D volume. The yellow arrow points to an immobilized phage on a cluster of resistant cells. Note that phages are much smaller than the minimum resolvable volume of a confocal fluorescence microscope like that used here; as a result of this effect and the fact that their Alexafluor-633 tag is very bright, the phages appear larger than their true size.

571 **Supplemental Information:**

572

573 **Supplemental Materials and Methods** – Details of methodology for development of simulation
574 framework and experimental techniques used in the paper

575

576 **Supplemental Table S1** – List of parameters used for simulations, including references where applicable.

577

578 **Supplemental Figures 1-6.** Additional data in support of the main text.

579

580 **Supplemental Videos**

581

582 **SI Video 1:** A video illustrating the clearance of almost all susceptible cells (red) by phage (black)
583 infection. This occurs when resistant cells (blue) are initially rare in the population. This video is the
584 extended time series from which frames were taken for Figure 1B of the main text.

585

586 **SI Video 2:** A video illustrating the sequestration of phages (black) by majority resistant cell clusters
587 (blue), protecting most of the minority susceptible cell population (red) from phage exposure. This occurs
588 when resistant cells are initially common in the biofilm population. This video is the extended time series
589 from which frames were taken for Figure 1C of the main text.

590

591 **SI Video 3:** A biofilm simulation in 3-dimensions illustrating the clearance effect by which susceptible
592 cells (red, infected cells shown in green), when common in the biofilm population relative to resistance
593 cells (blue), are mostly or entirely killed off by a propagating phage infection.

594

595 **SI Video 4:** A biofilm simulation in 3-dimensions illustrating the phage sequestration effect by which
596 susceptible cells (red, infected cells shown in green), when initially rare in the biofilm population, are
597 protected from phage exposure by the majority of resistant cell clusters (blue) in their surroundings, which
598 prevent phages from reaching susceptible hosts in which to infect and multiply.

599

600 **Supplemental Information**

601

602 **Biofilm structure promotes coexistence of phage-resistant and**
603 **phage-susceptible bacteria**

604

605 Matthew Simmons^{1,2†}, Matthew C. Bond^{2†}, Britt Koskella³, Knut Drescher^{4,5}, Vanni Bucci^{1*}, Carey D.
606 Nadell^{2*}

607

608 ¹ Department of Bioengineering, Program in Biotechnology and Biomedical Engineering, University of
609 Massachusetts Dartmouth, N. Dartmouth, MA 02747, USA

610

611 ² Department of Biological Sciences, Dartmouth, Hanover, NH 03755, USA

612

613 ³ Department of Integrative Biology, University of California, Berkeley, Berkeley, CA 94720, USA

614

615 ⁴ Max Planck Institute for Terrestrial Microbiology, D-35043 Marburg, Germany

616

617 ⁵ Department of Physics, Philipps-Universität Marburg, D-35032 Marburg, Germany

618

619 ⁶ Department of Microbiology and Physiological Systems, University of Massachusetts Medical School,
620 Worcester, MA 01605, USA

621

622

623

624

625 † Co-first authors

626

627 * Authors for correspondence:

628

629 Carey Nadell (carey.d.nadell@dartmouth.edu)

630 Vanni Bucci (vanni.bucci2@umassmed.edu)

631

632 **Materials and Methods**

633 **Phage-biofilm modeling simulation framework:**

634 The simulation framework used for this study is an updated and expanded version of a modeling approach
635 developed in Simmons et al. (15). The major changes include a new implementation of bacteria as
636 individual particles rather than a homogeneous biomass, and a new implementation of phage diffusion,
637 detailed below. The simulations are built on a grid-based approach for tracking bacteria, phages, and solute
638 concentrations; spatial structure in the system is thus resolved at the level of grid nodes (which are $3\mu\text{m} \times$
639 $3\mu\text{m}$ for the simulations described in this paper). Within a grid node, bacteria and phages are tracked
640 individually but assumed to interact randomly. Using the FiPy partial differential equation solver for
641 Python (63), the same grid system is used to calculate nutrient diffusion from a bulk layer above the
642 biofilm toward the cell group surface, where it is consumed by bacteria (35, 37, 64).

643 As a result of nutrient consumption on the biofilm's advancing front (Figure 1A) nutrient gradients
644 are created with high nutrient availability in the outer cell layers and lower nutrient availability with
645 increasing depth into the biofilm interior. Cells near the liquid interface grow maximally, while cells
646 deeper in the biofilm interior grow relatively slowly. Fluid flow is modeled implicitly; following prior
647 literature, we allow the biofilm to erode along its outer front at a rate proportional to the square of the
648 distance from the basal substratum (described in detail in Simmons et al. (15)). Further, any phages that
649 depart from the biofilm into the surrounding liquid are advected out of the simulation space within one
650 iteration cycle, which is approximately 7-8 minutes in simulation time (see below).

651 The simulation framework was written in an object-oriented style. A simulation object is defined
652 *via* the space of the system, number and properties of implemented grid node containers, biological
653 behaviors of bacteria and phages, one-time events (e.g. phage pulse), and simulation exit conditions.
654 Briefly, the space of the system specifies physical information such as physical size and length scale of
655 the grid node array in which cells, phages, and solutes are implemented. The containers hold the
656 information about each modeled individual present in the system. Behaviors describe a container's
657 interactions with anything else including other containers, space, or time. Events are one-time-use include
658 the inoculation of the system with bacteria or pulses of phages into the simulation space.

659
660 Simulations were initiated by first defining the types of container contents, including both bacterial
661 strains/species of interest (phage-susceptible and phage-resistant), phage-infected bacteria, phages, and
662 the growth substrate as a solute. This process includes specifying values for basic biological and physical
663 parameters in the system (e.g. bacterial growth rate, phage infection rate per host-virus contact, phage lag
664 time, phage burst size, nutrient diffusivity, and others; the full list of parameter values and their
665 measurement origins is provided in Table S1). After containers are established in each simulation instance,
666 the simulation proceeds through inoculation of the two bacterial species on the substratum. Phages were
667 not introduced at the outset of simulations but rather at a set time after bacteria were permitted to grow,
668 as described in the main text. Simulations proceed along the following cycle of steps:

- 669 1. diffusion of the nutrient substrate,
- 670 2. biomass growth and division,
- 671 3. lysis of infected bacteria,
- 672 4. erosion of biomass,
- 673 5. phage movement,
- 674 6. detachment of biomass,
- 675 7. phage infection,
- 676 8. biofilm relaxation ('shoving'),
- 677 9. detachment of bacteriophage.

678

679 **Phage mobility implementation:** All processes describing phage-bacteria dynamics are equivalent to
680 those presented in Simmons et al. (15) with one exception pertaining to the methods of computing phage
681 entry and exit from the biofilm bacterial volume. This new approach is described in detail below.

682 Previously, we analytically solved the diffusion equation to approximate the phage density as a
683 function of location in the biofilm. Here, in order to accommodate for possible biological heterogeneity
684 in bacteriophage dynamics (65, 66), we introduced an algorithm for calculating phage movement by
685 modeling each phage's individual Brownian motion as a random walk. To account for the effect of the
686 biofilm matrix on phage movement, we introduced a new model parameter (the interaction rate, I)
687 controlling the diffusivity of phages through areas of simulation space occupied by bacterial biomass (15).
688 We also introduce a rate of removal (δ_p) which accounts for the removal of the phage due to the advection
689 of the system during the phage's motion through the space off of the biofilm, scaling with the square of
690 the distance away from the biofilm. There is an additional implicit advective removal of bacteriophage at
691 the end of the iteration (step 9 above) where any phages remaining off biofilm are removed from the space
692 via advection.

693 The improved implementation of phage mobility operates as follows. For each phage: We first
694 calculate the number of potential steps that could be taken in the next time interval as: $n =$
695 $D_p dt / (2 dl^2)$, and the time of these steps as $dt_p = 2 dl^2 / D_p$, where dl is the grid length scale, D_p is
696 the diffusivity of the phage, and dt is the simulation time step. Next for each step in n : 1) If the phage is
697 off the biofilm, determine whether the phage is removed from advection with probability $p = 1 -$
698 $e^{-dt_p d^2 \delta_p}$, where d is the distance away from the biofilm. 2) Next choose a target node by randomly
699 choosing direction. The probability to remain in the current grid node depends on the number of
700 dimensions (See calculation of phage diffusion properties, below). 3) Determine whether the phage is
701 able to diffuse into the target grid location with probability $p = 1 - e^{-dt_p \sum I_t + I_s}$, where I_t is the interaction
702 rate at the target grid node, and I_s is the interaction rate at the source node, and we sum over all biomass
703 in those nodes. 4) Finally, if the phage has interacted with biomass, cease motion. If it has not, move the
704 phage to the target grid node. As the interaction rate, I , increases, the ability of the phage to diffuse through
705 biomass decreases (e.g., p tends to 1), which is a per-individual-phage representation of the phage
706 impedance parameter previously described by Simmons et al. (15). Once the phage stops moving, we
707 evaluate the remaining time as $dt \times s/n$, where s is the number of steps taken, from 0 to n , and use it in
708 the infection step.

709

710 **Calculation of phage diffusion properties:** The model for an individual phage taking a step across the
711 grid nodes is that it must diffuse a large enough distance from a grid node. The unnormalized probability
712 density of diffusing within in one place can be described by the solution of the diffusion equation in radial
713 coordinates: $e^{-r^2/(a dt_p D_p)}$. Here r indicates the distance away from the starting point, a is a constant
714 indicating dimension: $a = 1$ for two dimensions and $a = 4$ for three dimensions, while other terms are
715 explained above. To get the probability of remaining in a radius ρ , we integrate from $0 \rightarrow \rho$ over r with a
716 normalization factor which is an integration over all space ($\int_0^\infty e^{-r^2/(a dt_p D_p)}$). Letting $\rho = \frac{dl}{\sqrt{\pi}}$ gives a
717 circle whose area is equal to the area of a grid node, and noting that $dt_p = 2 dl^2 / D_p$, the integration
718 yields $\text{erf}(\frac{1}{\sqrt{2 a \pi}})$, or $p = 0.42$ in two dimension and $p = 0.22$ in three dimensions.

719

720 **Details on simulation initial conditions and execution of parameter sweeps:** Where possible,
721 biological and physical parameters of the simulation system were constrained according to experimentally

722 measured values for *E. coli* and phage T7, which were the focal species of our experiments as well (see
723 Table S1). Following our previous biofilm dynamics simulation work (15, 38, 67), each simulation starts
724 with an initial ratio of phage-susceptible and -resistant strains on the solid substratum, and these two
725 strains compete for access to space and growth-limiting nutrients that diffuse from a bulk layer above the
726 biofilm. When the biofilm height reaches $30\mu\text{m}$, (approximately 7 days for the lowest condition and 1
727 day for the highest), a pulse of bacteriophages to the highest point of susceptible biomass, simulating an
728 individual cell bursting, releasing bacteriophages. Repeating our simulation parameter sweeps with earlier
729 ($20\mu\text{m}$ biofilm height) or later ($50\mu\text{m}$ biofilm height) phage inoculation had no effect on the qualitative
730 outcomes. Two phage inoculation methods were tested. The first approach to phage inoculation was a
731 120-virion pulse at a single position at highest point of susceptible biomass in the biofilm. The second
732 was a “spray” of phages in the area just above the biofilm outer surface: 300 phages are added to randomly
733 selected grid nodes $9\mu\text{m}$ above the biofilm. Data reported in Figure 1 correspond to simulations obtained
734 using the first method, but we confirmed that the core results are upheld when using the “spray” method
735 of phage inoculation.

736 Simulations were run until one of two different exit conditions was reached: either susceptible or
737 resistant cells going to fixation, or the simulation ran to a pre-specified end point (time of infection + 10
738 days). Simulations were run for 21 different nutrient bulk values corresponding to an approximate time
739 of infection at 1 through 7 days, where the faster growth has slightly greater strain mixing (68, 69). The
740 initial resistant strain frequency also varied from 1% to 99% in 21 steps. Additional simulations were run
741 also for three distinct fitness cost levels of phage resistance, and for three different values of the interaction
742 rate parameter I , which effectively varied phage mobility through biofilms easily penetrating the biofilm
743 surface to severely impeded immediately upon biofilm contact (see main text). We ran 100 simulations
744 with different random seeds to completion for each combination of parameters in the main text.
745 Simulations which had a maximum number of phages in any particular iteration of less than 150 were
746 excluded from the analysis, resulting in over 90 simulations for each set in the main text. For the well-
747 mixed control simulations, we disabled all spatially dependent behaviors: substrate diffusion, biomass
748 erosion, biofilm detachment, biofilm relaxation, phage detachment.

749
750

751 **Experimental Materials and Methods:**

752 **Bacterial Strains.** Both strains used in this study are *E. coli* AR3110 derivatives, created using the lambda
753 red method for chromosomal modification (70). The ΔtrxA deletion strain was created by amplifying the
754 locus encoding chloramphenicol acetyltransferase (*cat*) flanked by FRT recombinase sites target sites,
755 using primers with 20bp sequences immediately upstream and downstream of the native *trxA* locus. The
756 FRT recombinase encoded on pCP20 was used to remove the *cat* resistance marker after PCR and
757 sequencing confirmed proper deletion of *trxA*. The wild type *E. coli* AR3110 was engineered to
758 constitutively express the fluorescent protein mKate2, and the *trxA* null mutant was engineered to
759 constitutively produce the fluorescent protein mKO- κ . These fluorescent protein expression constructs
760 were integrated in single copy to the *attB* locus on the chromosome, and they allowed us to visualize the
761 two strains and distinguish them in biofilm co-culture by confocal microscopy.

762

763 **Biofilm growth in microfluidic channels.** Microfluidic devices were constructed by bonding poly-
764 dimethylsiloxane (PDMS) castings to size #1.5 36mm x 60mm cover glass (ThermoFisher, Waltham MA)
765 (71, 72). Bacterial strains were grown in 5mL lysogeny broth overnight at 37°C with shaking at 250 r.p.m.
766 Cells were pelleted and washed twice with 0.9% NaCl before normalizing to $\text{OD}_{600} = 0.2$. Strains were
767 combined in varying ratios (see main text) and inoculated into channels of the microfluidic devices.

768 Bacteria were allowed to colonize for 1 hour at room temperature (21-24°C) before providing constant
769 flow (0.1µL/min) of Tryptone broth (10g L⁻¹). Media flow was achieved using syringe pumps (Pico Plus
770 Elite, Harvard Apparatus) and 1mL syringes (25-gauge needle) fitted with #30 Cole palmer PTFE tubing
771 (ID = 0.3mm). Tubing was inserted into holes bored in the PDMS with a catheter punch driver.
772

773 **Bacteriophage amplification and purification.** T7 phages (23) were used for all experiments. *E coli*
774 AR3110 was used as the phage host for amplification. Purification was conducted according to a protocol
775 developed by Bonilla et al. (73). Briefly, overnight cultures of AR3110 were back diluted 1:10 into 100mL
776 lysogeny broth supplemented with 0.001 M CaCl₂ and MgCl₂, and incubated for 1 hour at 37°C with
777 shaking; phages from a frozen stock were inoculated and incubated until the culture cleared completely
778 as assessed by eye. Cultures were pelleted, sterile filtered and treated with chloroform. Chloroform was
779 separated from lysate *via* centrifugation and aspiration of supernatant. Phage lysate was then concentrated
780 and cleaned using phosphate buffered saline and repeated spin cycles of an Amicon® Ultra centrifugal
781 filter units with an Ultracel 200kDa membrane (Millipore Sigma, Burlington MA). Purified phages were
782 stored at 4°C.
783

784 **Bacteriophage labeling.** Phage labeling began with a high titer phage prep (2x10¹⁰ PFU/mL) produced
785 using the method described above. 900µL of the phage prep was combined with 90µL sodium bicarbonate
786 (1M, pH = 9.0) and 10µL (1mg/mL) amine reactive Alexa-633 probe (ThermoFisher, Waltham MA) and
787 incubated at room temperature for 1 hour. In this manner the phages were conjugated to dye non-
788 specifically at one or more locations on their capsid coats. Labeled phage were then dialyzed against 1L
789 phosphate buffered saline to remove excess dye using a Float-A-Lyzer®G2 Dialysis Device MWCO 20kD
790 (Spectrum Labs, Rancho Dominguez CA). Labeled phage were diluted in Tryptone broth (10gl⁻¹) to
791 working concentration (2x10⁷ PFU/mL) prior to use.
792

793 **Phage-biofilm microfluidic experiments.** Biofilms consisting of varying ratios of susceptible and
794 resistant cells were grown in microfluidic devices for 48 hours at room temperature (21-24°C) under
795 constant media flow (tryptone broth 10gl⁻¹ at 0.1µL/min). Biofilms were imaged immediately prior to
796 phage treatment to establish exact starting ratios of wild type cells (phage-susceptible) and *trxA* deletion
797 mutants (phage-resistant). Subsequently, inlet media tubing was removed from the PDMS microfluidic
798 device and new tubing containing phage diluted in tryptone broth (2x10⁷ PFU/mL at 0.1µL/min) was
799 inserted. Phage treatment continued for 1 hour, after which original tubing was reinserted to resume flow
800 of fresh tryptone broth without phages. Biofilms were imaged approximately 6, 12, 24 and 48 hours after
801 the conclusion of the phage treatment until a population dynamic steady state was reached.
802

803 **Imaging and quantification procedures.** Biofilms were imaged using a Zeiss LSM 880 confocal
804 microscope with a C-Apochromat 10X/0.45 water objective or a 40X/1.2 water objective. A 594-nm laser
805 was used to excite mKate2, and a 543-nm laser line was used to excite mKOκ. A 640-nm laser was used
806 to excite Alexafluor 633. Whole chamber Z stacks were acquired by utilizing 1x10 vertical tile scans (total
807 rectangular area ~500x5000µm). Quantification of biomass was performed using customized scripts in
808 MATLAB (MathWorks Natick, MA) as previously described in Drescher et al. 2014 (74) and Nadell et
809 al. 2015 (75).
810

811
812 **Supplementary Table S1: Model Parameters used for Simulations**

Parameter	Value used in the simulations	Description	References where applicable	Representative value ranges and additional references, where applicable
x_{max}, y_{max}	900 μm , 150 μm	The physical size of the system	N/A	-
dl, dV	3 μm , 27 μm^3	Length and volume of a grid element	N/A	-
N_{max}	1.1 – 8 $mg L^{-1}$	Maximum density of substrate (range of values investigated in this study)	(76)	-
N_{max}	0.055 – 0.4 $mg L^{-1}$	Well-mixed simulation nutrient availability	(77)	-
D_N	$2.3 * 10^{-6} cm^2 s^{-1}$	Diffusivity of substrate	(76)	-
h	15 μm	Diffusion boundary layer height		-
K_N	1.18 $mg L^{-1}$	Half saturation constant for substrate	(35, 78)	5 - 225 Biofilm heterotrophic bacterial biomass, including fecal coliforms, e.g. <i>E. coli</i> (78, 79) 4.86 <i>Pseudomonas putida</i> F1 on glucose (80)
δ_E	20 $(m h)^{-1}$	Erosion constant	(36)	-
m_s	$10^{-12} g$	Bacterial mass per cell	(81)	10^{-12} <i>E. coli</i> DSM 613
μ_s (*)	14.1 day^{-1}	Maximum growth rate	(82)	17.8 <i>E. coli</i> K-12 on glucose (83) 4.8-17.6 <i>E. coli</i> K-12 on different substrates (84) 6.1 Wastewater heterotrophic bacterial

				biomass (85)
S_{max}	200 g L^{-1}	Maximum active biomass density	(86)	-
Y	0.495	Yield of substrate converted to biomass	(67)	0.69-0.77 Wastewater bacteria (87) 0.41 <i>E. coli</i> K-12 on glucose (83) 0.41-0.51 <i>P. putida</i> F1 on glucose (80)
β	120	Phage burst size	(8, 88)	Bacteriophage T7
D_p	$3.82 * 10^{-7} \text{ cm}^2 \text{ s}^{-1}$	Phage diffusivity constant	This Study	Bacteriophage T7
I	$0.067 - 0.12 (m_s \mu\text{m}^3)^{-1} \text{ s}^{-1}$	Rate of interaction of phage particles with biomass particles	This study	-
δ_p	$0.001 - 10 (\mu\text{m}^2 \text{ h})^{-1}$	Phage removal rate	(8, 88)	-
τ	28.8 minutes	Incubation period before lysis	(15)	Bacteriophage T7
γ	2.92 h^{-1}	Infection rate per biomass per phage		-

813

814

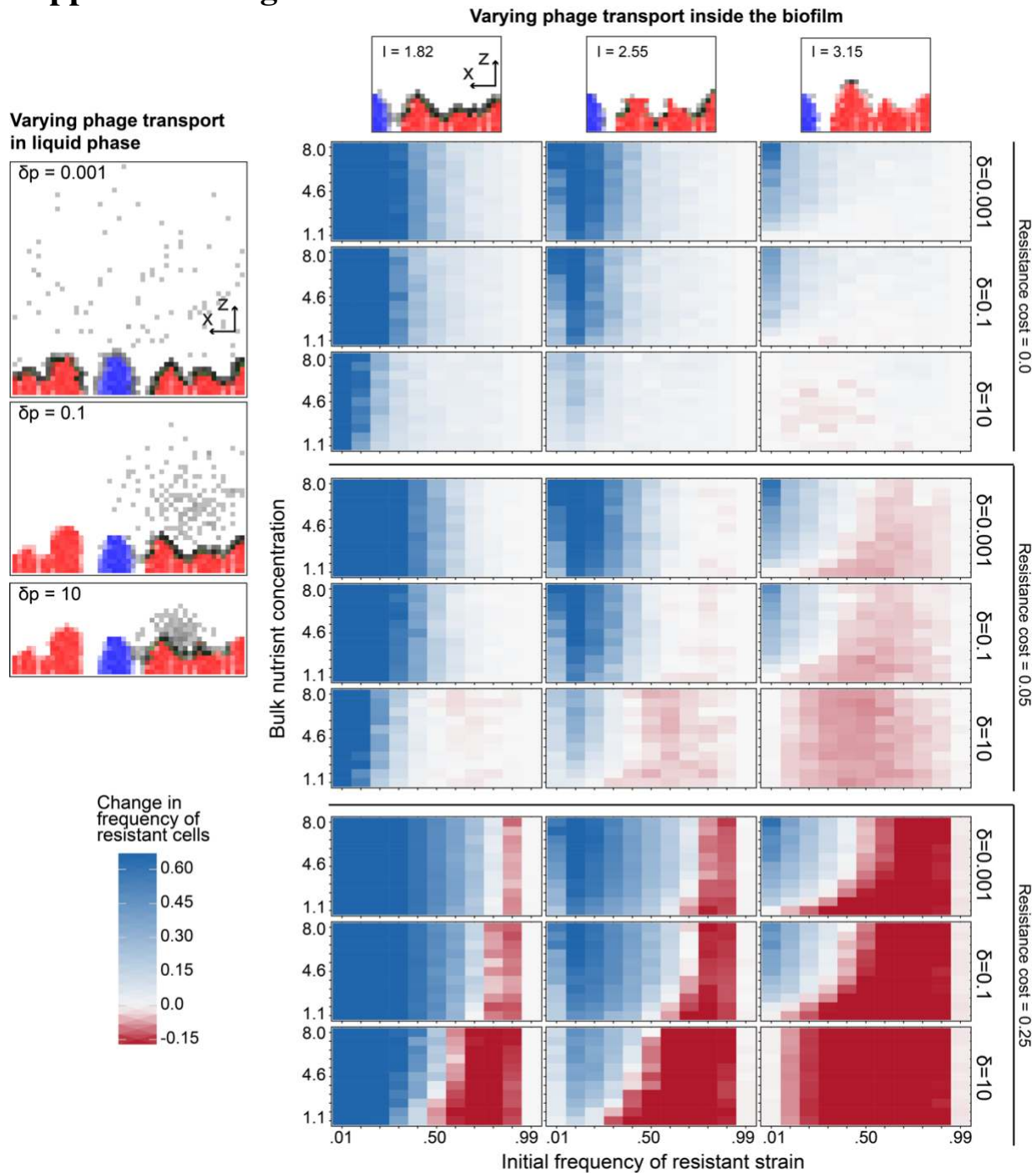
815 (*) The max growth rate is determined from the model equations as $\mu_s = q_s Y$. q_s is the substrate uptake

816 rate with value 28.5 g day^{-1} as in Lapidou et al. (82)

817

818

819 Supplemental Figures



820
821 **Figure S1. Parameter sensitivity analysis for predicted coexistence of phage-resistant and phage-**
822 **susceptible cells.** The robustness of the predictions outlined in the main text were tested with variation in
823 the cost of phage resistance, the diffusivity of phages through biofilm biomass, and the speed of phage
824 transport/removal in the liquid phase outside of biofilms. As in Figure 1 of the main text, for each
825 parameter combination, simulations were run for a range for varying initial strain frequency, and for
826 varying bulk nutrient concentration, which controls the bacterial growth rate. The heatmaps depict the
827 change in frequency of the resistant strain after phage exposure.

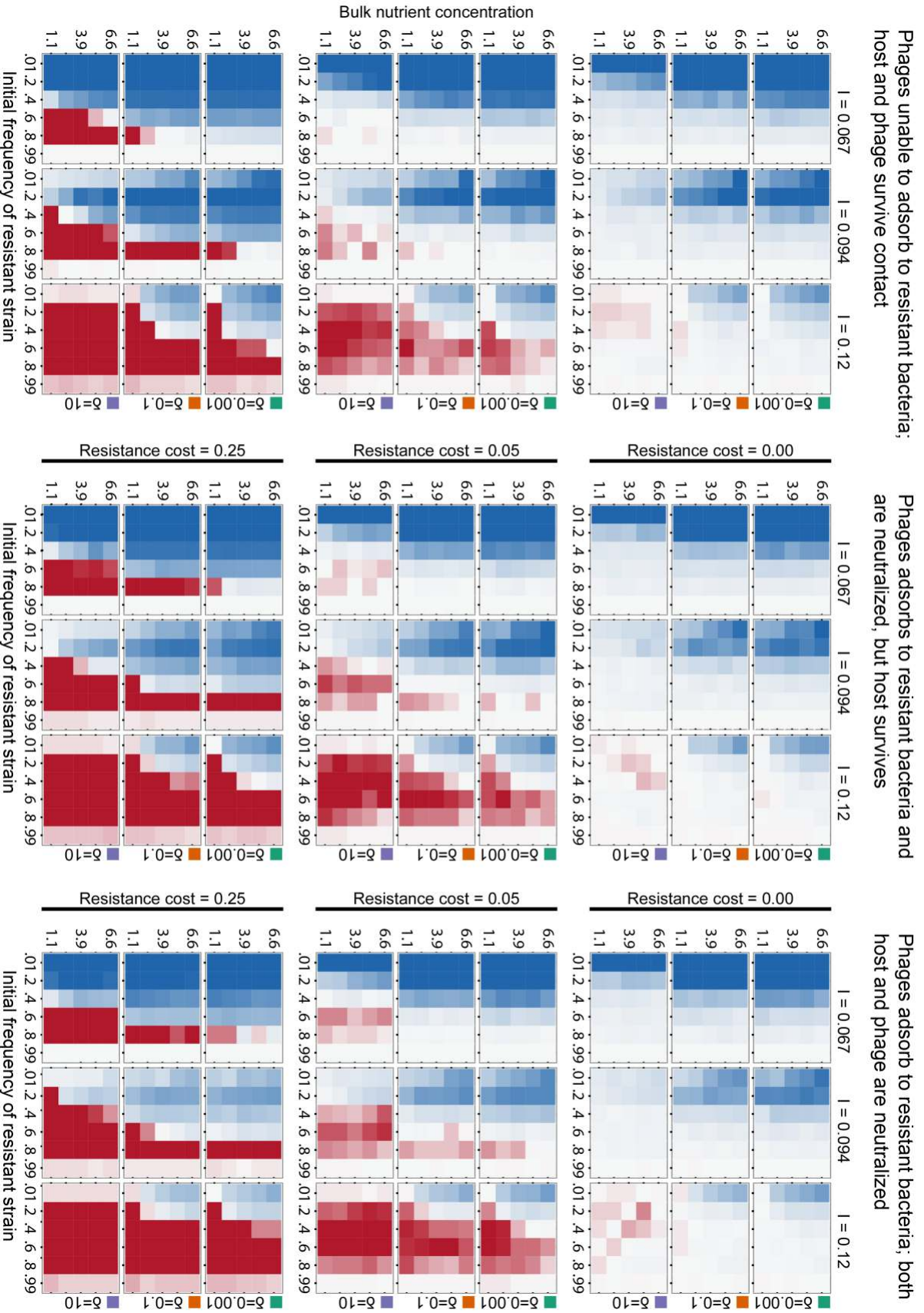
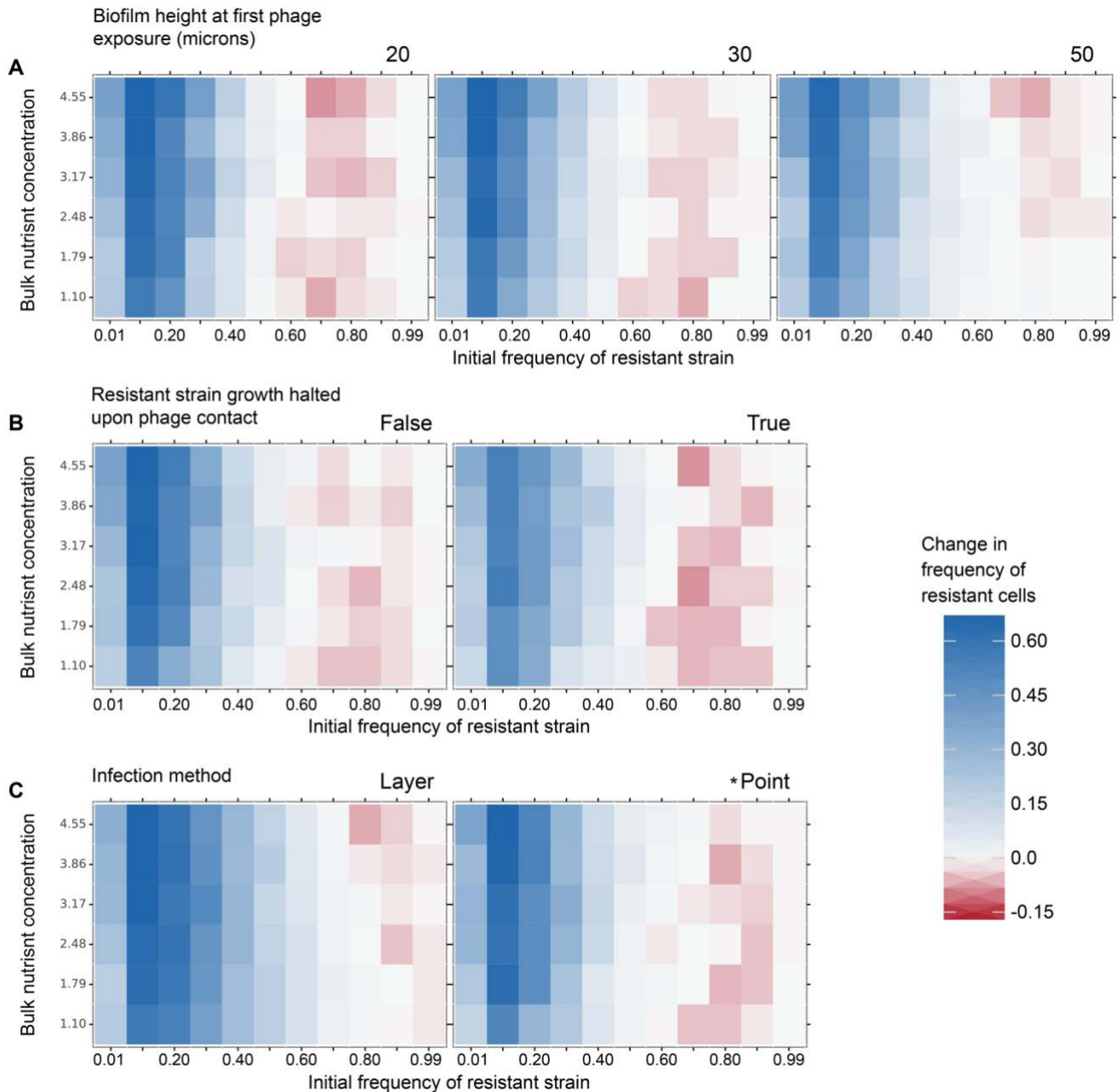


Figure S2. The mechanism of phage resistance does not substantially impact patterns of selection for resistance in biofilms.

Here the parameter sweep analysis shown in Figure S1 was repeated (at one quarter resolution) for three different mechanisms of phage resistance on the part of resistant hosts. At left, phages cannot adsorb to hosts, as could be the case for mutants that have lost the phage receptor. In center, phages can adsorb to resistant hosts and re neutralized, but the host survives the encounter and remains viable, as could be the case for CRISPR-Cas9 based resistance to phages. Finally, for comparison we repeat at right the analysis of phage resistance in which both the host and the phage are neutralized by the contact event. This condition represents the abortive infection resistance mechanism that is implemented in our experimental system (see Main Text).



829

830

831

832

833

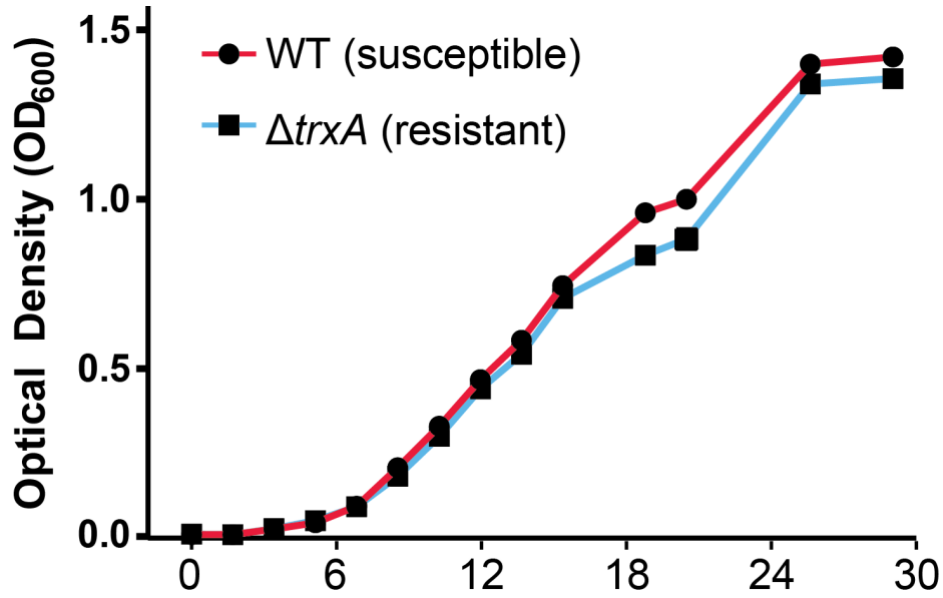
834

835

836

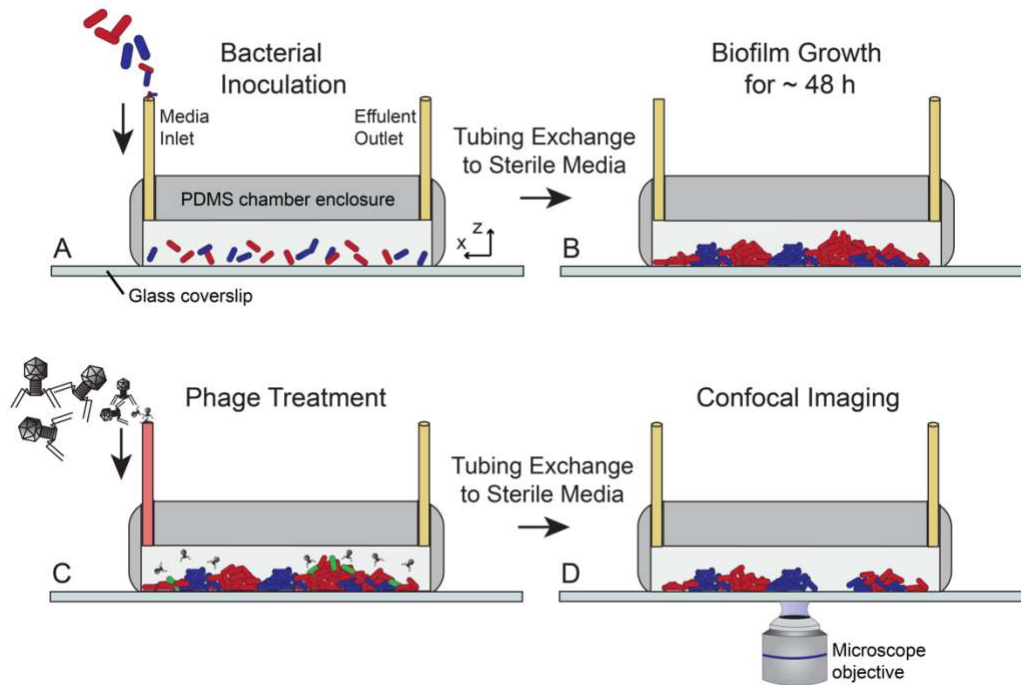
837

Figure S3. Extended simulations testing the robustness of negative frequency dependent selection for phage resistance. In addition to core simulation parameters assessed in figure S1, we also tested for the robustness of our results against (A) variation in the threshold biofilm height at which phages were pulsed into the system, (B) whether or not resistant cell growth halts upon phage contact, which is the case for some forms of phage resistance that do not permit phage amplification but still allow phage entry into the host cell, and (C) whether phages were introduced in an even layer across the biofilm upper surface, or at a single point on the biofilm surface. All other parameter in these simulations are the same as those used for simulations summarized in Figure 1 of the main text.



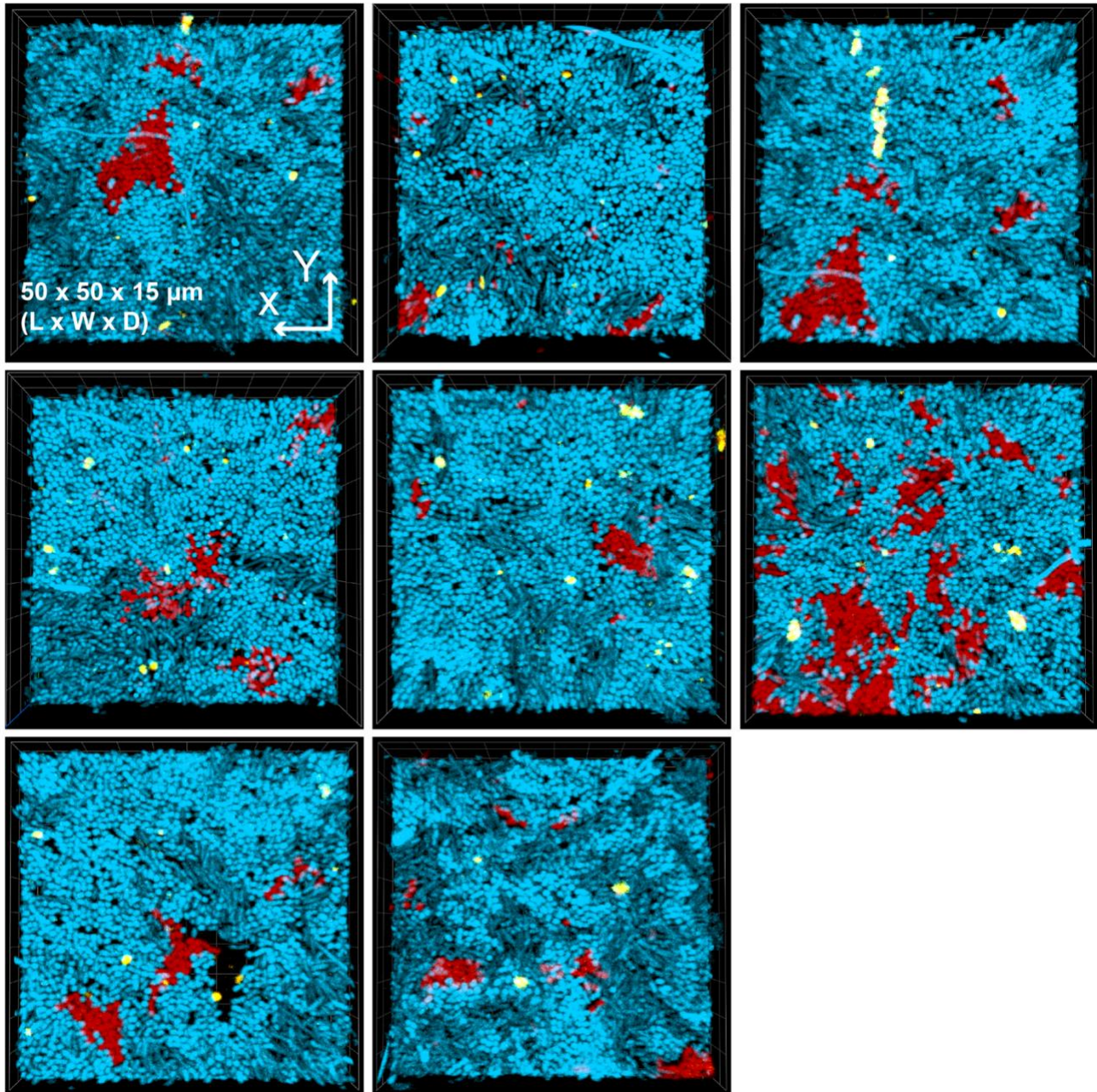
838

839 **Figure S4. Growth curves of *E. coli* wild type AR3110 (phage T7-susceptible, blue) and Δ *trxA***
840 **mutants (phage T7-resistant, red) in tryptone liquid culture with shaking at 30°C.** Data points denote
841 mean values of 6 total runs of the experiment. Fitting each run to the logistic growth equation yielded an
842 average maximum growth rate of $0.40 \pm 0.004 \text{ h}^{-1}$ for the phage-susceptible WT, and a maximum growth
843 rate of $0.37 \pm 0.002 \text{ h}^{-1}$ for the phage-resistant Δ *trxA* mutant.
844



845
846
847
848
849
850
851
852
853

Figure S5. Diagram of experimental biofilm growth and phage treatment regime. (A) Biofilms were grown by inoculating phage-susceptible and -resistant cells in controlled ratios (see main text) onto the glass bottom of PDMS microfluidic devices. (B) Biofilms were grown in the absence of phage for 48 hours, after which (C) the medium inlet tubing was switched to perfuse biofilms with T7 phages. (D) the inlet tubing was replaced again to continue flow of fresh media, and image series were acquired by confocal microscopy.



854
855 **Figure S6. Phages (yellow) trapped by majority resistant bacteria (blue) are unable to reach and**
856 **infect sparse patches of susceptible cells (red).** Additional replicates of the experiment depicted in
857 Figure 4 of the main text, in which biofilms inoculated with 20:1 resistant-susceptible cells were grown
858 for 48 hours and then pulsed with phages for prior to imaging by confocal microscopy. Each panel above
859 is a 3-D biofilm volume rendering $\sim 50\mu\text{m} \times 50\mu\text{m} \times 15\mu\text{m}$ [L x W x D]. Note that the top-left panel is a
860 recapitulation of Figure 4 for comparison with other replicates.
861